RESEARCH ARTICLE

The variability and interdependence of spider viscid line tensile properties

Gracia Belén Perea , Gustavo R. Plaza , Gustavo V. Guinea , Manuel Elices , Beatriz Velasco and José Pérez-Rigueiro

SUMMARY

True stress–true strain curves of naturally spun viscid line fibres retrieved directly from the spiral of orb-webs built by *Argiope trifasciata* spiders were measured using a novel methodology. This new procedure combines a method for removing the aqueous coating of the fibres and a technique that allows the accurate measurement of their cross-sectional area. Comparison of the tensile behaviour of different samples indicated that naturally spun viscid lines show a large variability, comparable to that of other silks, such as major ampullate gland silk and silkworm silk. Nevertheless, application of a statistical analysis allowed the identification of two independent parameters that underlie the variability and characterize the observed range of true stress–true strain curves. The combination of this result with previous mechanical and microstructural data suggested the assignment of these two independent effects to the degree of alignment of the protein chains and to the local relative humidity, which, in turn, depends on the composition of the viscous coating and on the external environmental conditions.

Key words: biomaterials, silk, flagelliform silk.

INTRODUCTION

Variability plays an ambivalent role in the performance of biological materials and, more specifically, in the performance of spider silk fibres. It is assumed that the possibility of spinning fibres within a vast range of tensile properties allows adaptation of the material to the immediate requirements of the spider (Madsen et al., 1999; Madsen and Vollrath, 2000), which would represent an obvious evolutionary advantage (Blackledge et al., 2012). The finding of organs and structures in the spider's spinning system that allow varying of the stresses exerted on major ampullate gland silk during its formation and, in turn, its tensile behaviour (Gosline et al., 2002; Ortlepp and Gosline, 2004) has clarified the possible mechanism by which spiders might exert this control on the mechanical properties of this material. In contrast to its advantageous biological function, variability represents a major drawback for the characterization and subsequent analysis of silk, as a large variability in nominally similar fibres prevents the drawing of firm conclusions on most aspects of silk performance (Dunaway et al., 1995).

Consequently, analysing the variability of spider silk should be aimed at both understanding its origin and describing its extent in natural structures. The former is required for developing a sound experimental work to characterize the material, and establishing relationships between microstructure and properties, and the latter provides information on the range of properties demanded of silk in order to fulfil its biological function.

Among the silk types spun by spiders (Vollrath, 1992), viscid lines fibres are the elements that form the spiral in the Araneoidea lineage, and result from the combination of the fibres produced in the flagelliform gland and the viscous coating synthesized in the aggregate gland (Townley et al., 1991). The success of the design of a two-dimensional web with a capture spiral is indicated by the existence of over 10,000 species of Orbicularian spiders. Among them, the Araneoidea lineage, which is characterized by the use of viscid line fibres for building the capture spiral, comprises ~95% of the species in the group. The remaining 5% corresponds to the Deinopoidea lineage (Griswold, 1993; Griswold et al., 1998), which is characterized by the use of looped cribellar fibrils on the core flagelliform fibre instead of the aqueous coating of the viscid line.

Despite its widespread distribution in terms of both species and ecological niches, the available information on the mechanical behaviour of viscid lines is scarce (Blackledge and Hayashi, 2006; Gosline et al., 1993; Vollrath and Edmonds, 1989), especially if it is compared with the large amount of information available on major ampullate gland silk (Heim et al., 2009; Kaplan et al., 1991). The presence of the viscous coating is partly responsible for this lack of information, as it prevents the detailed characterization of the tensile properties of the core fibres; however, it is assumed that this somehow modulates the overall tensile behaviour of the viscid line (Edmonds and Vollrath, 1992; Vollrath and Edmonds, 1989).

The coating synthesized in the aggregate gland is composed of a combination of glycoproteins and smaller biomolecules, such as fatty acids in aqueous solution (Salles et al., 2006). This viscous coating provides an adhesive character that contributes to improve the entanglement ability of the web (Betz and Kölsch, 2004), and might play an even more active role in the capture process with the presence of toxins that would affect the prey and limit its chance to escape (Cesar et al., 2005; Marques et al., 2004; Opell et al., 2006). An additional role with deep implications in terms of the performance of the fibre has also been proposed for the viscous coating, based on the plasticizing effect of water on the tensile properties of silk (Gosline

et al., 1984; Work, 1977). In this regard, it is assumed that the presence of the coating leads to a local decrease of vapour pressure, so that water evaporation from the web due to the external environmental conditions is prevented (Vollrath et al., 1990), and the flagelliform fibre is maintained in a state of high hydration. This assumption is supported by the increase in plasticity associated with water uptake, which is not accompanied by an increase in the adhesion of the coating (Opell et al., 2011a; Opell et al., 2011b).

The development of a methodology for removing the viscous coating without damaging the flagelliform fibre (Guinea et al., 2010) represented a major advance in the characterization of this silk. In particular, it was shown that (1) flagelliform silk presents a ground state to which it can revert independently from the previous loading history of the fibre, and (2) clean fibres (i.e. without the viscous coating) presented a variability comparable to those of intact fibres (i.e. with the viscous coating). This second observation indicated that the presence of the coating could not be the only source of variability in this material. However, the continuation of the analysis was prevented by the absence of a reliable procedure to measure cross-sectional area and, consequently, to get an accurate determination of the mechanical properties in terms of stress–strain curves. Such a measuring procedure has been developed subsequently as presented in this work, so that a study of the variability shown by spider intact viscid line fibres (i.e. with the viscous coating) as retrieved directly from the web could be undertaken. The statistical analysis of the stress–strain curves shows their dependence on just two independent parameters, from which the experimental curves could be reconstructed in all cases. The combination of this finding with complementary results on the tensile properties of viscid lines (Guinea et al., 2010) gives insight on the origin of the observed variability. In particular, it is suggested that the tensile properties of viscid lines may be dependent on both the alignment of the protein chains and the local relative humidity to which the fibre is subjected.

MATERIALS AND METHODS
Obtaining viscid line fibres
Viscid line fibres were obtained from webs built in 0.8×0.8 m wooden frames by *Argiope trifasciata* spiders (Forskål 1775). Fibres of 50–70 mm length were retrieved between two consecutive radii in order to have at least two adjacent samples, so that the tensile properties and cross-sectional area could be measured. All samples retrieved from a single viscid line between two consecutive radii are adjacent, and it was found in a previous work (Guinea et al., 2010) that adjacent samples yield similar mechanical properties even in terms of force–displacement curves. Specimens were mounted in frames (Perez-Rigueiro et al., 1998) cut out of plastic sheets. Notation and labelling of silk fibres are shown in Fig. 1. Sample labelling follows the order: web sector, sector step (batch) and step segment (sample). Forty-five samples from 11 different webs built by four different spiders were used in this study.

Cross-sectional area measurement
At least one fibre from each step (batch) was used to measure its cross-sectional area. The measured area was used to compute the mechanical properties of all the segments of the batch, as it has been shown that adjacent samples have concurring mechanical properties. Cross-sectional cuts of the fibres were prepared by ultramicrotomy. Samples were mounted in plastic frames and stained by covering the fibre with a drop of Richardson's Methylene Blue stain. Samples were heated at 70°C until the drop dried, and the excess Methylene Blue was removed with distilled water. The fibre was allowed to dry overnight. Staining allows the identification of the fibre during ultramicrotomy, as the low contrast between the fibre and the embedding resin in the optical microscope represents a major difficulty during the ultramicrotomy of silk samples.

The stained fibre was placed on a previously prepared Spurr resin base in a silicone embedding mould (SPI Supplies, West Chester,
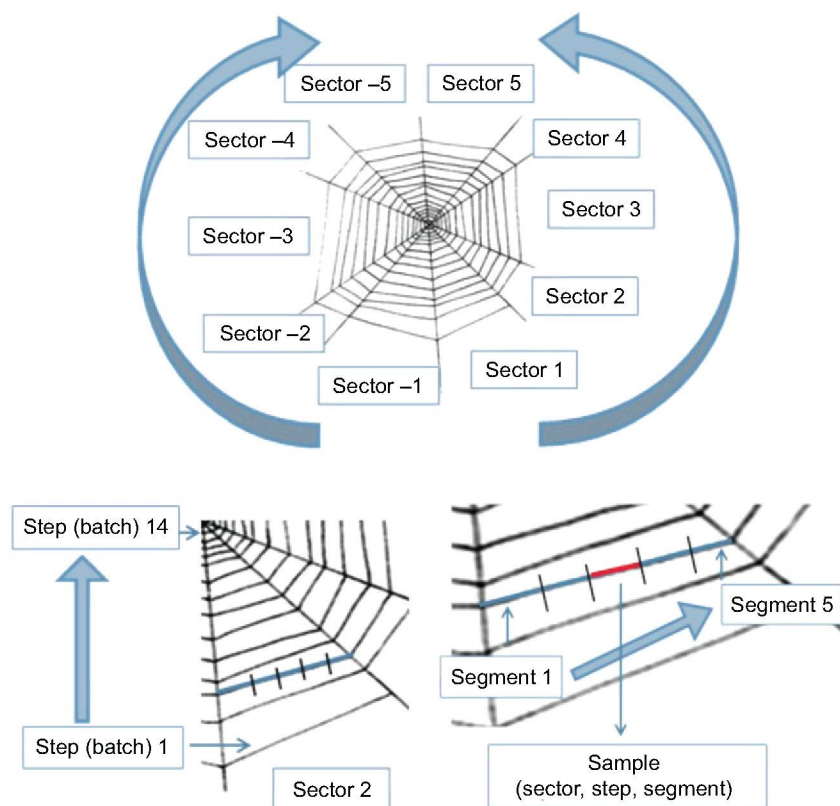

Fig. 1. Scheme of an orb web illustrating the code used for the identification of the samples with three integers (sector, step, segment). Adjacent samples were obtained from the viscid line fibres between two consecutive radii.

PA, USA) and covered with Spurr resin. This resin–silk–resin sandwich was cured at 70°C for 72 h. The resin block was cut to approximately its middle with a manual saw and the surface containing the silk fibres was polished to obtain a flat surface as smooth as possible. Initial cuts were performed in a Leica Ultracut UCT ultramicrotome with glass knife, with a facet angle of 6 deg and cross-section of 5–10 μm. Final sections of 60–90 nm thickness were cut with a diamond knife with a facet angle of 6 deg in a Sorvall Ultra Microtome MT500. It has been found that this process can be used with native (i.e. non-cleaned) samples; however, it is more efficient if samples are first subjected to a cleaning step. Removal of the coating proceeded by centrifugation as described elsewhere (Guinea et al., 2010).

Samples were metallized with gold, and observed in a scanning electron microscope (SEM-JEOL 6300), at 10 kV and $I=0.06$ nA. The cross-sectional area was computed from the cross-sectional areas as observed in the micrographs using the ImageJ program. Examples of micrographs showing the cross-sections of viscid lines are given in Fig. 2 with the coating intact (Fig. 2A) or after removal of the coating by the centrifugation step (Fig. 2B).

Tensile tests

Intact viscid line fibres mounted on plastic frames with a typical base length of 5 mm were tensile tested in an Instron 3309-622/8501 (Instron, Canton, MA, USA) appended to an environmental chamber (Dycometal CCK-25/300, Barcelona, Spain) (Guinea et al., 2003). The value of the base length was chosen as a compromise between the requirement of obtaining a sufficient number of samples from each web, and the necessity to minimize the errors associated with uncertainties related to the initial length of the fibre, in particular for the calculation of strain. An optical extensometer (Keyence LS-7500/LA 7030M, Itasca, IL, USA) with a resolution of 0.2 μm was used for measuring the deformation of the fibre. Forces were measured with a 100 mN load cell with 0.1 mN resolution (HBM 1-Q11, Darmstadt, Germany). Tensile tests proceeded at 20°C and 35% relative humidity (RH) with a displacement speed of 1 mm min^{-1}.

The cross-sectional areas were used to compute true stress (σ)–true strain (ε) curves of the adjacent fibres from the force–displacement data. True stress was computed under the hypothesis of constant volume, a usual hypothesis for silks that was proved for the major ampullate silk (MAS) gland (Guinea et al., 2006).

The constant volume hypothesis implies that:

$$A_0 L_0 = A L , \qquad (1)$$

where A_0 is the initial cross-sectional area, measured from the SEM micrographs, L_0 is the initial length, A is the instantaneous area and L is the instantaneous length of the fibre.

The true stress (σ) and true strain (ε) are given by the expressions:

$$\sigma = \frac{F}{A} ,$$

$$\varepsilon = \ln\left(\frac{L}{L_0}\right). \qquad (2)$$

Data analysis

Analysis of the data followed a previous study in which the variability of *A. trifasciata* MAS fibres (Garrido et al., 2002) was assessed, and consisted of the following steps. (1) Selection of an initial arbitrary set of parameters that allow the true stress–true strain curves to be described. In this case, the initial set of parameters included the values of stress at the following strains: 10% ($\sigma_{10\%}$),
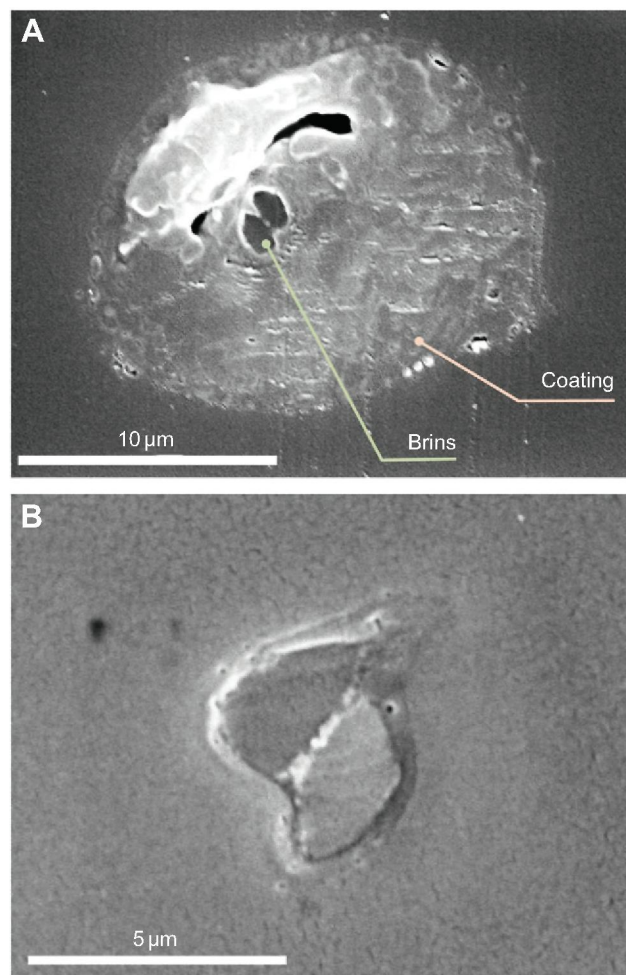
Fig. 2. Scanning electron microscope (SEM) micrographs used for computing the cross-sectional areas of flagelliform fibres. (A) Fibre not subjected to the cleaning step. The coating can be clearly identified surrounding the flagelliform fibres. (B) Fibre subjected to the cleaning step. The two brins that make up the fibre can be clearly observed in both cases.

20% ($\sigma_{20\%}$), 30% ($\sigma_{30\%}$), 40% ($\sigma_{40\%}$), 50% ($\sigma_{50\%}$), 60% ($\sigma_{60\%}$) and 70% ($\sigma_{70\%}$). No particular choice was implied in the initial set of parameters, except that it allowed a sufficiently accurate reconstruction of the experimental curve. (2) Statistical analysis to determine the dependence or independence among the parameters. (3) Determination of a functional dependence between the dependent parameters. (4) Determination of a suitable functional form for the stress–strain curve. (5) Reconstruction of the experimental curve from the set of independent parameters using the functional dependence found in 4.

RESULTS AND DISCUSSION
Mechanical behaviour

Representative force–displacement curves from several samples retrieved from two different webs are shown in Fig. 3. The large variability characteristic of silks is apparent both within a single web and between webs. In order to determine whether this variability might simply reflect differences in the cross-sectional area of the fibres, the true stress–true strain curve of each sample was calculated from the measured cross-sectional area of an adjacent sample. As indicated above, adjacent fibres yield concurring force–displacement
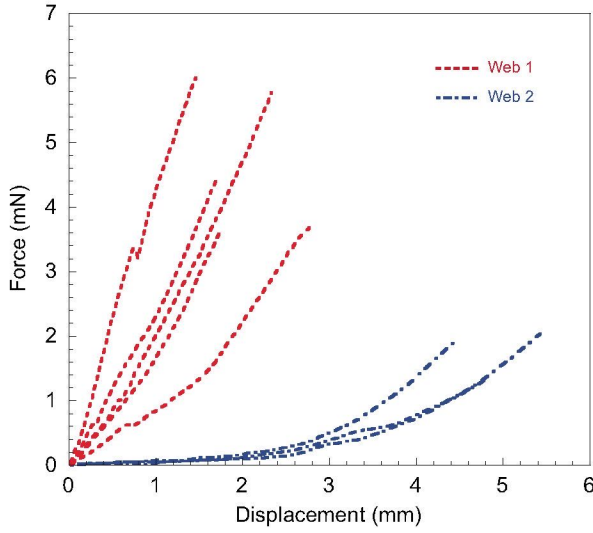
Fig. 3. Force–displacement curves of intact viscid line fibres retrieved from two different webs.
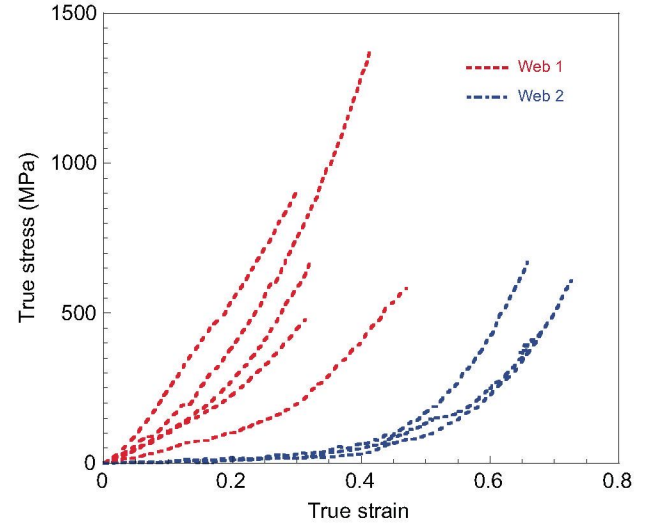

Fig. 4. True stress (σ)–true strain (ε) curves of the same samples presented in Fig. 3.

curves, which renders support to this methodology. Measurement of cross-sectional area revealed large variations both between samples from different webs (minimum value: 2.8 μm²; maximum value: 16.6 μm²) and between samples retrieved from a single web (minimum value: 4.3 μm²; maximum value: 11.5 μm²).

True stress–true strain curves corresponding to the samples shown in Fig. 3 are presented in Fig. 4. It can be seen that the use of exact measurements of cross-sectional area for calculating stresses does not lead to an improvement in the reproducibility of the tensile properties. Consequently, it is concluded that intrinsic differences must exist between the fibres that account for the observed variability.

Statistical analysis
Parameterization of stress–strain curves

Following the methodology described above, the first step of the statistical analysis requires defining a set of parameters that allow reconstruction of the true stress–true strain curves with sufficient accuracy. The initial set of parameters for describing the stress–strain curve was taken as: $\sigma_{10\%}$, $\sigma_{20\%}$, $\sigma_{30\%}$, $\sigma_{40\%}$, $\sigma_{50\%}$, $\sigma_{60\%}$ and $\sigma_{70\%}$. This set of parameters was arbitrarily chosen with the only condition that it allows a sufficiently accurate reconstruction of the experimental curves by approximating, for instance, the curve by a series of straight segments between each two consecutive parameters of the set.

Dependence/independence of the mechanical parameters

The statistical dependence/independence of each pair of the initial set of parameters was assessed through the χ^2-test of independence (Brandt, 1998; Garrido et al., 2002). The χ^2-test of independence requires calculation of the function:

$$X^2 = \sum_{i=1}^{k}\sum_{j=1}^{l}\frac{\left(n_{ij} - Np_iq_j\right)^2}{Np_iq_j}, \tag{3}$$

where N is the total number of tensile tests, k is the number of intervals into which the range of values of the first parameter is divided, l is the number of intervals into which the range of values of the second parameter is divided, and n_{ij} is the number of tensile tests for which the first parameter lies in the interval i and the second parameter lies in the interval j. The values of each parameter were

typically distributed into six or seven intervals, in order to allow a sufficient number of values to be included in each interval.

p_i and q_j are defined as follows:

$$p_i = \frac{1}{N}\sum_{j=1}^{l}n_{ij},$$

$$q_j = \frac{1}{N}\sum_{i=1}^{k}n_{ij}. \tag{4}$$

The independence test proceeds by comparing the value of X^2 with the tabulated value of the $\chi_{1-\alpha}^2$ function. The number of degrees of freedom for $\chi_{1-\alpha}^2$ is given by the product $(k-1)(l-1)$, and the level of significance α is assigned a value of 5% in keeping with common practice (Garrido et al., 2002). If $X^2 > \chi_{1-\alpha}^2$, the independence hypotheses has to be rejected; if $X^2 < \chi_{1-\alpha}^2$, the independence hypothesis cannot be rejected. The results of the independence test are presented in Table 1, from which it is apparent that the number of independent parameters can be reduced to two. The limit between the two ranges of the independent set of parameters can be established at approximately $\sigma_{40\%}$. Consequently, it is concluded that the intrinsic variability observed in the tensile properties of viscid lines is the result of two independent mechanisms.

Determination of a functional dependence between the dependent parameters

The next step of the statistical analysis is the determination of a functional dependence between the parameters that are found to be dependent from the χ^2-test of independence. Fig. 5 shows representative results obtained for pairs of dependent (Fig. 5A) and independent (Fig. 5B) parameters. As can be seen in Fig. 5B, the distribution of values of independent parameters corresponds to a cloud of scattered points that do not show any functional dependence. In contrast, the distribution of values for the dependent parameters could be approximated by straight lines in all cases, as illustrated in Fig. 5A. This result allows the set of initial parameters with which the curve can be reconstructed to be reduced to just two, which are used as reference parameters. The linear dependence between the parameters of each subset of independent parameters allows selection of any pair of parameters as long as one is chosen from each subset. For the following analysis, the values of $\sigma_{20\%}$ and $\sigma_{50\%}$

Table 1. Results of applying the χ^2-test of independence to the parameters chosen to describe the true stress–true strain curves of viscid line fibres

	$\sigma_{20\%}$	$\sigma_{30\%}$	$\sigma_{40\%}$	$\sigma_{50\%}$	$\sigma_{60\%}$	$\sigma_{70\%}$
$\sigma_{10\%}$	124,78 (>26,3) dependent	110,67 (>26,3) dependent	264,64 (>31,41) dependent	17,99 (<26,3) independent	19,25 (<26,3) independent	9,56 (<31,41) independent
$\sigma_{20\%}$		129,63 (>26,3) dependent	126,97 (>26,30) dependent	38,05 (<51,00) independent	35,62 (<43,77) independent	10,13 (<16,92) independent
$\sigma_{30\%}$			75,99 (>26,30) dependent	25,08 (<26,30) independent	13,48 (<26,30) independent	13,5 (<16,92) independent
$\sigma_{40\%}$				71,31 (>26,3) dependent	36,83 (>26,3) dependent	16,41 (<26,30) independent
$\sigma_{50\%}$					41,90 (>26,3) dependent	12,00 (>9,49) dependent
$\sigma_{60\%}$						17,10 (>16,92) dependent

The following strains were used: 10% ($\sigma_{10\%}$), 20% ($\sigma_{20\%}$), 30% ($\sigma_{30\%}$), 40% ($\sigma_{40\%}$), 50% ($\sigma_{50\%}$), 60% ($\sigma_{60\%}$) and 70% ($\sigma_{70\%}$).
The number on the left corresponds to the statistical estimator X^2 and the number on the right (in parentheses) corresponds to the tabulated value of the χ^2 function for a level of significance of $\alpha=5\%$. $X^2>\chi^2$ implies that the independence hypothesis between the two parameters has to be rejected.

where chosen as reference parameters, although the forthcoming analysis is independent of this choice.

Determination of a suitable functional form for the true stress–true strain curves

Three possible functional forms were explored to account for the experimental true stress–true strain curves: second-order polynomial, third-order polynomial and exponential with an independent term. It was found that the second-order polynomial provided a poor agreement with the experimental values, and although the third-order polynomial provided a good agreement in most cases, it did not allow fitting for a few. Finally it was found that an exponential function with an independent term:

$$\sigma = b\,(e^{a\varepsilon} - 1)\,,\qquad(5)$$

where σ stands for the true stress and ε for the true strain, reproduced with sufficient accuracy all the experimental data. The choice of an exponential form has additional support from theoretical studies of the scaling effect of the interactions in the tensile properties of viscid lines (Zhou and Zhang, 2005; Becker et al., 2003).

Reconstruction of true stress–true strain curves

Ultimate validation of the previous analysis requires that the experimental curves can be reconstructed from the minimum set of parameters established as $\sigma_{20\%}$ and $\sigma_{50\%}$. The reconstruction process requires the calculation of the values of the parameters a and b that appear in Eqn 5. Using the values of the two independent parameters chosen as reference parameters to reconstruct the true stress–true strain curve, $\sigma_{20\%}$ and $\sigma_{50\%}$, the values of a and b are obtained from:

$$\sigma_{20\%} = b\,(e^{a0.2} - 1)\,,\qquad(6)$$

$$\sigma_{50\%} = b\,(e^{a0.5} - 1)\,,\qquad(7)$$

which yields the following implicit equation:

$$a = 2\ln\left[1 + \frac{\sigma_{50\%}}{\sigma_{20\%}}\left(e^{a0.2} - 1\right)\right].\qquad(8)$$

Solving for a in Eqn 8 with a numerical method allows calculation of the parameter b from the equation:

$$b = \frac{\sigma_{50\%}}{\left(e^{a0.5} - 1\right)}\,,\qquad(9)$$

which completes the reconstruction process.

Fig. 6 compares the experimental curves presented in Fig. 4 with those calculated using the reconstruction method from the values of the parameters $\sigma_{20\%}$ and $\sigma_{50\%}$. The concurrence of the reconstructed and the experimental curves renders support for the statistical analysis performed above.

The statistical analysis of true stress–true strain curves on its own does not provide information by which the ultimate deformational mechanisms underlying the variability observed in viscid line fibres might be identified, but establishes severe restrictions to their total number. Thus, the results presented above demonstrate that the origin of the variability observed in natural viscid lines can be traced back to two independent effects. However, the identification of these fundamental mechanisms requires the use of additional mechanical and microstructural information.

In this context, it was found (Guinea et al., 2010) that water content influences the tensile properties of viscid line silk by comparing the tensile properties of flagelliform fibres (i.e. viscid lines without the adhesive coating) at different values of RH. The effect of water was especially evident at low strains, with a change of the elastic modulus of almost two orders of magnitude being determined by varying RH from 10% to 100% (immersion in water). These results suggest that water content (or, equivalently, local RH) might be one of the two independent mechanisms that control the performance of the fibre.

Comparison of the tensile properties exhibited by clean flagelliform and MAS fibres suggests that the second mechanism could be assigned to the different alignment of the protein chains among different samples. In particular, it has been found that the whole range of tensile properties of MAS fibres can be obtained predictably and reproducibly by a simple process consisting of stretching the fibres in water from the initial maximum supercontracted state to a pre-determined value of strain (Guinea et al., 2005). This effect has been interpreted as the result of varying the degree of alignment of the proteins with respect to the macroscopic axis of the fibre. The concurrent behaviour of clean flagelliform and MAS fibres when tested in water and, specifically, the existence of a maximum supercontracted state in both materials clearly supports this assignment as the second independent source of variability in viscid line fibres.

The identification of a ground state (i.e. maximum supercontracted state) and the likely influence of the alignment of the proteins on the mechanical performance of the fibres lead to the question of what the values of these parameters might be in the naturally spun material. The combined application of the
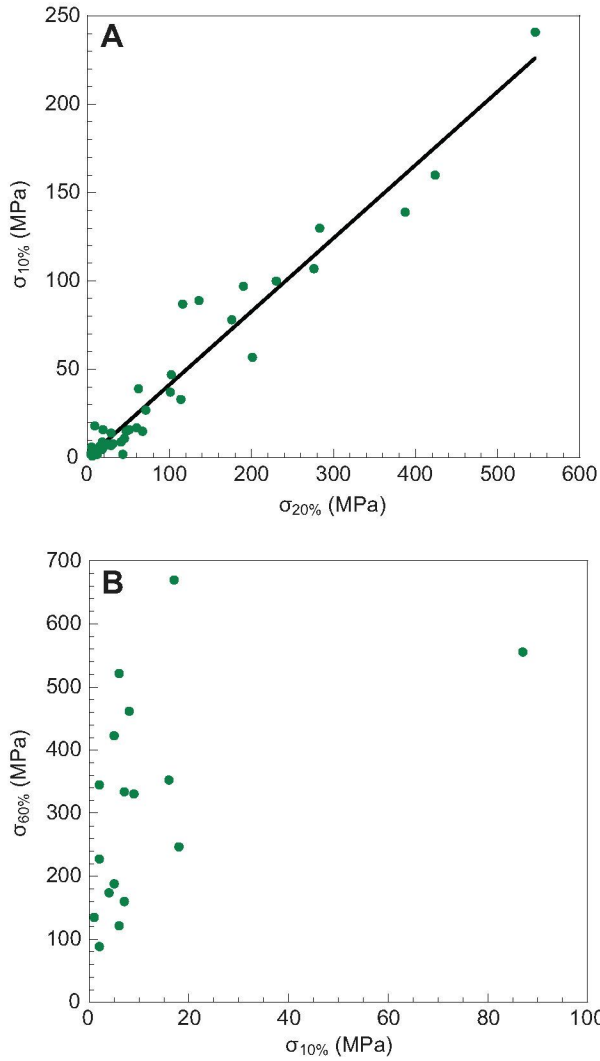
Fig. 5. Distribution of the pairs of stresses (A: $\sigma_{10\%}$, $\sigma_{20\%}$; and B: $\sigma_{60\%}$, $\sigma_{10\%}$) as obtained from tensile tests. The straight line in A is the result of a linear regression analysis. No clear correlation can be established between the values of $\sigma_{60\%}$ and $\sigma_{10\%}$, consistent with the statistical analysis of independence.

Fig. 6. Comparison of the experimental true stress(σ)–true strain (ϵ) curves (broken lines) and reconstructed stress–strain curves (solid lines) for the two different webs presented in Fig. 4.

cleaning procedure and the similar behaviour shown by adjacent fibres allows calculation of the percentage of supercontraction (%SC) of intact viscid lines (i.e. with the adhesive coating) in the web as:

$$\%\mathrm{SC} = \frac{L_0 - L_{\mathrm{MS}}}{L_{\mathrm{MS}}}, \qquad (10)$$

where L_0 is the initial length of the intact (i.e. with the viscous coating) viscid line and L_{MS} is the length of an adjacent sample subjected to maximum supercontraction. Application of this equation to the fibres analysed in this study yields a value of %SC=40±15%, with a maximum value of 56% and a minimum value of 26%. These results indicate a considerable degree of alignment of viscid line fibres, when spun to build the orb-web.

CONCLUSIONS

The study of the mechanical properties of viscid line spider silk reveals a large variability, even between fibres produced under nominally comparable conditions. The development of a
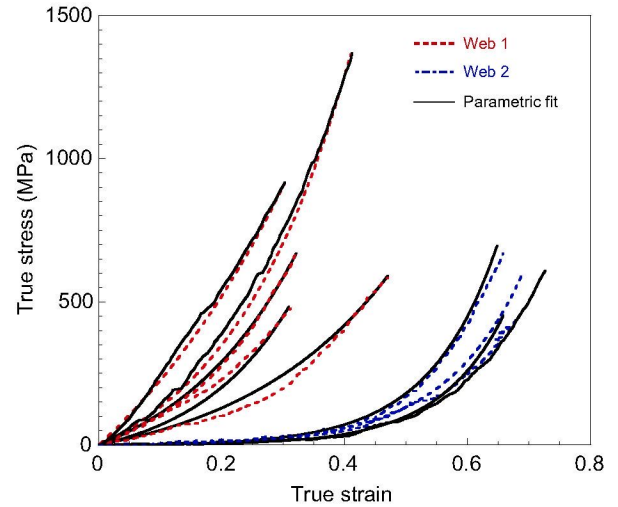
methodology that allows (1) removal of the aqueous coating produced by the aggregate gland and (2) accurate measuring of the cross-sectional area of the fibres led, for the first time, to a significant number of true stress–true strain curves being obtained for naturally spun viscid line fibres.

The availability of a sufficient number of true stress–true strain curves allowed us to undertake a statistical study that parallels previous analyses on *A. trifasciata* MAS fibres. In particular, the minimum number of independent parameters that allow reconstruction of the experimental curves was determined from a χ^2-statistical analysis of independence. This number was found to be two, as supported by the concurrence of the experimental and reconstructed true stress–true strain curves in all cases.

Combining these observations with previous mechanical and microstructural data suggests that the mechanisms that determine the tensile properties of viscid line fibres could be assigned to (i) the degree of alignment of the protein chains with respect to the macroscopic axis of the fibre and (ii) to the local relative humidity, which, in turn, depends on the adhesive coating and environmental conditions. Whether the spider exerts a similar active control on viscid line fibres by controlling either or both mechanisms, as demonstrated in *A. trifasciata* MAS, remains an open question.

AUTHOR CONTRIBUTIONS

J.P.R. proposed the experiments and wrote the main text. G.B.P. prepared the material and conducted the mechanical tests, assisted by B.V. G.V.G., M.E. and G.R.P. contributed to the data analysis and reviewed the manuscript.

COMPETING INTERESTS

No competing interests declared.

REFERENCES

Becker, N., Oroudjev, E., Mutz, S., Cleveland, J. P., Hansma, P. K., Hayashi, C. Y., Makarov, D. E. and Hansma, H. G. (2003). Molecular nanosprings in spider capture-silk threads. *Nat. Mater.* **2**, 278-283.

Betz, O. and Kölsch, G. (2004). The role of adhesion in prey capture and predator defence in arthropods. *Arthropod Struct. Dev.* **33**, 3-30.

Blackledge, T. A. and Hayashi, C. Y. (2006). Silken toolkits: biomechanics of silk fibers spun by the orb web spider *Argiope argentata* (Fabricius 1775). *J. Exp. Biol.* **209**, 2452-2461.

Blackledge, T. A., Pérez-Rigueiro, J., Plaza, G. R., Perea, B., Navarro, A., Guinea, G. V. and Elices, M. (2012). Sequential origin in the high performance properties of orb spider dragline silk. *Sci. Rep.* **2**, 782.

Brandt, S. (1998). *Statistical and Computational Methods in Data Analysis.* New York, NY: Springer Verlag.

Cesar, L. M. M., Mendes, M. A., Tormena, C. F., Marques, M. R., de Souza, B. M., Saidemberg, D. M., Bittencourt, J. C. and Palma, M. S. (2005). Isolation and chemical characterization of PwTx-II: a novel alkaloid toxin from the venom of the spider *Parawixia bistriata* (Araneidae, Araneae). *Toxicon* **46**, 786-796.

Dunaway, D. L., Thiel, B. L. and Viney, C. (1995). Tensile mechanical property evaluation of natural and epoxide-treated silk fibers. *J. Appl. Polym. Sci.* **58**, 675-683.

Edmonds, D. T. and Vollrath, F. (1992). The contribution of atmospheric water-vapor to the formation and efficiency of a spiders capture web. *Proc. R. Soc. B* **248**, 145-148.

Garrido, M. A., Elices, M., Viney, C. and Perez-Rigueiro, J. (2002). The variability and interdependence of spider drag line tensile properties. *Polymer (Guildf.)* **43**, 4495-4502.

Gosline, J. M., Denny, M. W. and Demont, M. E. (1984). Spider silk as rubber. *Nature* **309**, 551-552.

Gosline, J. M., Pollak, C. C., Guerette, P. A., Cheng, A., Demont, M. E. and Denny, M. W. (1993). Elastomeric network models for the frame and viscid silks from the orb web of the spider *Araneus diadematus. Silk Polymers* **544**, 328-341.

Gosline, J., Lillie, M., Carrington, E., Guerette, P., Ortlepp, C. and Savage, K. (2002). Elastic proteins: biological roles and mechanical properties. *Philos. Trans. R. Soc. B* **357**, 121-132.

Griswold, C. E. (1993). Investigations into the phylogeny of the Lycosoid spiders and their kin (Arachnida: Araneae: Lycosoidea). *Smithson. Contrib. Zool.* **539**, 1-39.

Griswold, C. E., Coddington, J. A., Hormiga, G. and Scharff, N. (1998). Phylogeny of the orb-web building spiders (Araneae, Orbiculariae: Deinopoidea, Araneoidea). *Zool. J. Linn. Soc.* **123**, 1-99.

Guinea, G. V., Elices, M., Perez-Rigueiro, J. and Plaza, G. (2003). Self-tightening of spider silk fibers induced by moisture. *Polymer (Guildf.)* **44**, 5785-5788.

Guinea, G. V., Elices, M., Pérez-Rigueiro, J. and Plaza, G. R. (2005). Stretching of supercontracted fibers: a link between spinning and the variability of spider silk. *J. Exp. Biol.* **208**, 25-30.

Guinea, G. V., Pérez-Rigueiro, J., Plaza, G. R. and Elices, M. (2006). Volume constancy during stretching of spider silk. *Biomacromolecules* **7**, 2173-2177.

Guinea, G. V., Cerdeira, M., Plaza, G. R., Elices, M. and Pérez-Rigueiro, J. (2010). Recovery in viscid line fibers. *Biomacromolecules* **11**, 1174-1179.

Heim, M., Keerl, D. and Scheibel, T. (2009). Spider silk: from soluble protein to extraordinary fiber. *Angew. Chem. Int. Ed. Engl.* **48**, 3584-3596.

Kaplan, D. L., Lombardi, S., Muller, W. S. and Fossey, S. A. (1991). *Biomaterials. Novel Materials from Biological Sources,* 53pp. New York, NY: Stockton Press.

Madsen, B. and Vollrath, F. (2000). Mechanics and morphology of silk drawn from anesthetized spiders. *Naturwissenschaften* **87**, 148-153.

Madsen, B., Shao, Z. Z. and Vollrath, F. (1999). Variability in the mechanical properties of spider silks on three levels: interspecific, intraspecific and intraindividual. *Int. J. Biol. Macromol.* **24**, 301-306.

Marques, M. R., Mendes, M. A., Tormena, C. F., Souza, B. M., Ribeiro, S. P., Rittner, R. and Palma, M. S. (2004). Structure determination of an organometallic 1-(diazenylaryl)ethanol: a novel toxin subclass from the web of the spider *Nephila clavipes. Chem. Biodivers.* **1**, 830-838.

Opell, B. D., Bond, J. E. and Warner, D. A. (2006). The effects of capture spiral composition and orb-web orientation on prey interception. *Zoology* **109**, 339-345.

Opell, B. D., Schwend, H. S. and Vito, S. T. (2011a). Constraints on the adhesion of viscous threads spun by orb-weaving spiders: the tensile strength of glycoprotein glue exceeds its adhesion. *J. Exp. Biol.* **214**, 2237-2241.

Opell, B. D., Karinshak, S. E. and Sigler, M. A. (2011b). Humidity affects the extensibility of an orb-weaving spider's viscous thread droplets. *J. Exp. Biol.* **214**, 2988-2993.

Ortlepp, C. S. and Gosline, J. M. (2004). Consequences of forced silking. *Biomacromolecules* **5**, 727-731.

Perez-Rigueiro, J., Viney, C., Llorca, J. and Elices, M. (1998). Silkworm silk as an engineering material. *J. Appl. Polym. Sci.* **70**, 2439-2447.

Salles, H. C., Volsi, E. C. F. R., Marques, M. R., Souza, B. M., dos Santos, L. D., Tormena, C. F., Mendes, M. A. and Palma, M. S. (2006). The venomous secrets of the web droplets from the viscid spiral of the orb-weaver spider *Nephila clavipes* (Araneae, Tetragnatidae). *Chem. Biodivers.* **3**, 727-741.

Townley, M. A., Bernstein, D. T., Gallagher, K. S. and Tillinghast, E. K. (1991). Comparative study of orb web hygroscopicity and adhesive spiral composition in 3 araneid spiders. *J. Exp. Zool.* **259**, 154-165.

Vollrath, F. (1992). Spider webs and silks. *Sci. Am.* **266**, 70-76.

Vollrath, F. and Edmonds, D. T. (1989). Modulation of the mechanical-properties of spider silk by coating with water. *Nature* **340**, 305-307.

Vollrath, F., Fairbrother, W. J., Williams, R. J. P., Tillinghast, E. K., Bernstein, D. T., Gallagher, K. S. and Townley, M. A. (1990). Compounds in the droplets of the orb spiders viscid spiral. *Nature* **345**, 526-528.

Work, R. W. (1977). Dimensions, birefringences, and force-elongation behavior of major and minor ampullate silk fibers from orb-web-spinning spiders – effects of wetting on these properties. *Text. Res. J.* **47**, 650-662.

Zhou, H. J. and Zhang, Y. (2005). Hierarchical chain model of spider capture silk elasticity. *Phys. Rev. Lett.* **94**, 028104.